Soil Dynamics and Earthquake Engineering 212 (2027) 110659

Contents lists available at ScienceDirect

Soil Dynamics and Earthquake Engineering

journal homepage: www.elsevier.com/locate/soildyn

Robust optimisation of RC bridge seismic design considering ground motion suite variability

Soheil Soltanieh [a], Panagiotis E. Mergos [a,*], Andreas J. Kappos [b]

[a] Department of Civil Engineering, School of Science and Technology, City St George's, University of London, EC1V 0HB, United Kingdom

[b] Department of Civil & Environmental Engineering, Khalifa University of Science & Technology, Abu Dhabi, United Arab Emirates

ARTICLE INFO

Keywords:
Robust design optimisation
Performance-based seismic design
Reinforced concrete bridge piers
Ground motion variability
Surrogate seismic demand models

ABSTRACT

Robust design optimisation (RDO) of performance-based seismic design (PBSD) has been established as a rigorous approach for obtaining optimal solutions that are minimally sensitive to record-to-record (RTR) variability of ground motions used in nonlinear response history analysis (NLRHA). However, this method is not able to explicitly account for the suite-to-suite (STS) variability due to the epistemic uncertainties associated with ground motion selection, especially when each suite is selected and scaled based on the requirements of the seismic design codes currently in force. To account for this uncertainty, this paper proposes a novel formulation for robust optimisation, which explicitly accounts for ground motion suite variability. In this method, one objective is to minimise the dispersion in the probability of limit state violation due to STS variability and the other objective is to minimise the economic costs. To increase the computational efficiency of the proposed method, surrogate seismic demand models are developed and applied to assess the probability of limit state violation. The application of the proposed framework is demonstrated using a case study of a typical reinforced concrete (RC) highway bridge with cylindrical piers, and the ability of the RDO framework to account for the STS variability is discussed. Finally, the Pareto-optimal solutions obtained from the proposed approach are compared with those given by the conventional RDO approach.

1. Introduction

Reinforced concrete (RC) bridges are critical, yet resource-intensive, components of transportation networks, particularly in seismically active regions. Optimising material usage in RC bridges is essential not only to reduce costs associated with cement and steel but also to support global decarbonisation efforts by minimising the carbon footprint of these materials. However, applying these strategies in isolation may lead to designs that are highly sensitive to the uncertainties associated with seismic performance [1].

The seismic performance assessment of RC bridges is an active area of research. For example, recent studies [2–6] have focused on the nonlinear dynamic response of RC bridges under earthquake loading, considering different ground motion characteristics such as near-field and far-field excitations, as well as spatial variability and other record features influencing structural demand [2,3,6]. Nonlinear response history analysis (NLRHA) is widely adopted as the most accurate method for estimating seismic demands across different hazard levels. A key challenge associated with NLRHA is the selection of an appropriate suite of recorded or simulated ground motions [2].

Design codes such as *fib* Model Code (MC) 2010 [7], Eurocode 8 [8, 9], and ASCE 7 [10] recommend the use of a sufficiently large suite of natural ground motion records when employing NLRHA for seismic design. The inherent record-to-record (RTR) variability of these motions contributes greatly to the uncertainty in seismic design. Such uncertainty necessitates the use of probabilistic optimisation frameworks accounting for the variability in input parameters. Two of such methods, commonly used in seismic design, are reliability-based design optimisation (RBDO) and robust design optimisation (RDO) [11,12].

The primary aim of typical RBDO is to minimise an objective function (e.g., cost or weight) while enforcing reliability-based constraints, such as target values for the probability of limit state exceedance or a specified reliability index [13,14]. An alternative formulation of RBDO seeks to include the reliability measure as an optimisation objective. This approach is typically formulated as a multi-objective optimisation framework where probability of structural failure (non-performance), or reliability index, is optimised alongside a cost function, while satisfying a combination of deterministic and/or probabilistic constraints [15–17].

* Corresponding author.
E-mail address: panagiotis.mergos.1@citystgeorges.ac.uk (P.E. Mergos).

https://doi.org/10.1016/j.soildyn.2026.110659
Received 8 April 2026; Received in revised form 16 July 2026; Accepted 18 August 2026
Available online 4 September 2026

In a reliability analysis, failure probability is usually estimated via Monte Carlo Simulation (MCS), often with sampling, incorporating variations in both seismic demands and structural capacity.

In contrast, RDO typically focuses on the impact of stochastic variations in design parameters on the deviation of structural response at specific performance limit states. Lagaros and Fragiadakis [18] highlighted the importance of incorporating the dispersion in seismic demands as an objective function in RDO, subject to performance-based seismic design (PBSD) constraints. This approach addresses the random nature of input parameters by controlling the variability of the seismic response parameters. RDO has been formulated and applied in the seismic design of different structures, including RC bridges [19,20]. More recently, Soltanieh et al. [1] proposed an RDO framework for the seismic design of RC bridge piers, seeking for solutions that are least sensitive to RTR variability and uncertainties associated with structural parameters, while satisfying PBSD constraints.

While the above-mentioned methodologies follow different optimisation objectives, they are able to account for the aleatory uncertainties related to the ground motion RTR (intra-suite) variability. However, these methods per se do not explicitly account for the epistemic uncertainties associated with the ground motion selection variability, which may lead to suite-to-suite (STS) (inter-suite) variability [21,22]. Although both RTR and STS variabilities originate from the inherent variability of earthquake ground motions, STS variability reflects the uncertainty associated with estimating a design performance statistics using a suite with a finite (typically small) number of ground motions. Consequently, expected seismic performance of an optimal design may be sensitive to the ground motion suite selected by the designer to satisfy a set of selection criteria [23,24]. This variability partly arises due to the fact that seismic design codes, including Eurocode 8 [9], provide generalised, non-prescriptive guidelines that permit ground motion selection and scaling based on the minimum criteria such as site-specific seismological constraints and constant-amplitude scaling to code-defined spectrum. Therefore, two practitioners following the same code-based ground motion selection procedure may still select dissimilar suites of records. It must be noted that recent codes, such as the forthcoming Eurocode 8 [9], alternatively allow for more refined ground motion selection and scaling methods based on the uniform hazard spectrum (UHS) and conditional spectrum (CS) [25–27]. Despite the rigour of these methods, they are less frequently used in engineering practice, primarily due to their complexity [28–30]. In any case, the epistemic uncertainty associated with STS variability persists in the PBSD problems [22].

The present paper proposes a new formulation for RDO within the context of PBSD of RC ductile-pier bridges, explicitly accounting for the STS variability. The aim is to explore the space of design variables subject to code-defined PBSD safety constraints to identify design solutions that are (*i*) cost-effective and (*ii*) minimally sensitive to the STS variability. A two-objective optimisation problem is defined to minimise the economic costs and the dispersion in the probability of limit state violation (P_{viol}) induced by STS variability. Use of probability-based objectives to quantify performance robustness against input uncertainties has been motivated by various engineering applications of RDO [31,32]. However, this study presents the first formulation of RDO using such an objective for PBSD of bridge piers. Furthermore, this is the first study addressing the STS variability through a structural optimisation framework.

The application of the proposed RDO methodology is demonstrated for seismic design optimisation of a representative RC bridge case study with circular piers and monolithic deck-to-pier connection. The optimisation constraint functions are set based on the *fib* MC2010 requirements. For calculation of the robustness measure (i.e., deviation of P_{viol}), surrogate seismic demand models are generated to increase the computational efficiency of RDO using a limited, yet representative, set of simulations. A distinguishing feature of these models is their ability to explicitly predict the standard deviation of seismic demands at different seismic action levels defined in *fib* MC2010. Lastly, the Pareto-optimal solutions obtained from the proposed RDO framework of this study are compared with those resulted from the conventional RDO approach.

2. Proposed robust design optimisation (RDO) framework

2.1. Formulation

Prior to introducing the proposed framework, the conventional formulation of RDO is briefly reviewed. In the context of seismic design, the generic form of RDO can be expressed as a two-objective optimisation problem [1,18]:

$$\begin{aligned} \textit{Minimise:} &\quad [C(\boldsymbol{x}), \sigma_{\theta_{max}}(\boldsymbol{x})] \\ \textit{Subjected to:} &\quad g_r(\boldsymbol{x}) \leq 0 \qquad \boldsymbol{r} = 1 : n_c \\ \textit{Where:} &\quad \boldsymbol{x} = (x_1, x_2, \ldots, x_p) \end{aligned} \tag{1}$$

wherein $C(\boldsymbol{x})$ is the cost function and $\sigma_{\theta max}(\boldsymbol{x})$ is the standard deviation of seismic demand (e.g., drift or rotation demands) for the *design candidate* $\boldsymbol{x}$ with p independent *design variables*, subject to the optimisation *constraints* $g_r(\boldsymbol{x}) \leq 0$ ($r = 1$ *to* n_c), where n_c is the total number of constraints.

The aforementioned framework involves some limitations: (*i*) although it accounts for RTR variability within a single ground motion suite, it is not able to account for the design robustness against the STS variability, (*ii*) the objective function $\sigma_{\theta max}(\boldsymbol{x})$ can only measure the robustness at each limit state distinctly and does not represent a unified measure over all limit states simultaneously, and (*iii*) the objective function $\sigma_{\theta max}(\boldsymbol{x})$ only represents the dispersion in seismic demands due to input variables and does not account for the structural limit state violation (i.e., demand versus capacity) and its associated uncertainties. These limitations motivate the development of the RDO framework put forward in this study, which is formulated as a bi-objective optimisation problem as follows:

$$\begin{aligned} \textit{Minimise:} &\quad [C(\boldsymbol{x}), \sigma_{P_{viol}}(\boldsymbol{x})] \\ \textit{Subjected to:} &\quad g_r(\boldsymbol{x}) \leq 0 \qquad \boldsymbol{r} = 1 : n_c \\ \textit{Where:} &\quad \boldsymbol{x} = (x_1, x_2, \ldots, x_p) \end{aligned} \tag{2}$$

where the first objective is to minimise the cost function $C(\boldsymbol{x})$, and the second one is to minimise the standard deviation of the probability of limit state violation P_{viol} (denoted as σ_{Pviol}), which is introduced in the present study in order to quantify robustness to ground motion suite variability. The optimiser explores the design search space ($\boldsymbol{x}$) with p independent design variables to find a balance between the objectives $C(\boldsymbol{x})$ and σ_{Pviol} under the optimisation constraints $g_r(\boldsymbol{x})$. A trade-off will be made here between the conflicting objectives of cost-effectiveness and the sensitivity of P_{viol} with respect to variation in the selected suite of ground motions. The remainder of this section elaborates on each component of the optimisation problem.

2.2. Design variables

In sizing optimisation of RC bridges in seismic regions, cross-sectional dimensions and steel reinforcement ratios of the piers are the most common design variables [33,34]. Accordingly, the design variables $\boldsymbol{x}$ adopted in this study include the dimensions and steel reinforcement ratios, both longitudinal and transverse, of pier critical cross-sections. In the case of circular bridge piers, this can be expressed as $\boldsymbol{x} = (D, \rho_l, \rho_w)$ where D is the diameter, ρ_l is the longitudinal reinforcement ratio, and ρ_w is the transverse reinforcement ratio. All design variables are assumed discrete to align with construction practices. The description can be generalised to bridges with multiple piers by defining each parameter as a sub-vector that contains the corresponding properties of each pier, e.g., $D = (D_1, D_2, \ldots)$, allowing non-identical pier configurations to be represented.

2.3. Optimisation constraints

Two sets of code-based optimisation constraints $g_r(\boldsymbol{x})$ are defined, including structural detailing parameters (SDP) and PBSD constraints [35]. In this study, and in the context of relevance to practical design, these constraints are defined in accordance with *fib* MC2010 [7] a document that reflects the modern seismic design 'philosophy'. The SDP constraints include the minimum and maximum diameters of reinforcing bars, permissible spacing, and the lower and upper bounds of volumetric ratios for longitudinal and transverse reinforcement, among others. The PBSD constraints are primarily associated with the serviceability limit state (SLS) and the ultimate limit state (ULS). The SLS comprises two performance levels, including operational (OP) and immediate use (IU), and the ULS includes life safety (LS) and near collapse (NC), each reflecting different degrees of structural damage.

A quantitative description of the structural performance requirements associated with the seismic action levels specified in *fib* MC2010 is provided in Table 1. As shown in this table, for different levels of seismic action, the design safety is evaluated by comparing the mean of maximum chord-rotation demands at kth seismic action level, $\theta^{(k)}_{max,m}$, with the design values of chord-rotation capacities, $\theta^{(k)}_{c,d}$, at the corresponding limit state. The generic form of the PBSD constraint function at kth limit state, $g^{(k)}_r(\boldsymbol{x})$, can be expressed as Eq. (3).

$$\theta^{(k)}_{max,m} \leq \theta^{(k)}_{c,d} \Rightarrow \frac{\theta^{(k)}_{max,m}}{\theta^{(k)}_{c,d}} - 1 \leq 0 \quad where \quad \frac{\theta^{(k)}_{max,m}}{\theta^{(k)}_{c,d}} - 1 = g^{(k)}_r(\boldsymbol{x}) \tag{3}$$

This ensures that unsafe designs are avoided through the performance constraints imposed on each limit state and prevent the optimisation algorithm from favouring designs that exhibit robustness but are unsafe.

In Table 1, the yield chord-rotation θ_y is defined as the sum of flexural and shear deformations in addition to the slippage of the tension bars from their anchorage in the joints or the foundation, as proposed by Biskinis & Fardis [36]. For LS and NC limit state verifications, the plastic part of the maximum chord-rotation demands is compared with the plastic part of the characteristic chord-rotation capacity $\theta_{pl,uk}$ divided by the safety factors (γ^*_R) given in Table 1. The $\theta_{pl,uk}$ is estimated using mean chord-rotation capacity ($\theta_{pl,um}$) divided by the model uncertainty factor ($\gamma_{Rd} = 2$). The $\theta_{pl,um}$ is the sum of the inelastic curvature along the plastic length at the end section and the post-yield part of fixed-end rotation due to slippage of longitudinal reinforcement from the anchorage zone [37]. The uncertainty factor γ_{Rd} is to convert $\theta_{pl,um}$ to the lower 5% fractile capacity [7]. The new Eurocode 8 [9] includes a new set of γ_{Rd} values, based on reliability-based calibrations reported in Ref. [38], which was not available at the time the present study was carried out.

In addition to the deformation-based constraints, the bridge pier is checked against the shear resistance of the plastic hinge V_{Rd} that reduces with increasing plastic rotation demands under seismic action [37]. The V_{Rd} is calculated based on Eurocode 8 [39], since it accounts for the reduction under cyclic loading and agrees well with the experimental resistance of numerous RC columns subject to cyclic tests in Ref. [40].

2.4. Objective functions

The first objective function is the cost of materials $C(\boldsymbol{x})$ of bridge piers, as shown in Eq. (4).

$$C(\boldsymbol{x}) = C_c(\boldsymbol{x}) + C_s(\boldsymbol{x}) \tag{4}$$

where C_c represents the cost of concrete, calculated by multiplying the concrete volume (m^3) by the unit cost of concrete (€/m^3). Similarly, C_s is the cost of reinforcing steel, determined by multiplying the total mass of steel reinforcement (kg) by its unit cost (€/kg). For simplicity, this paper focuses solely on the RC material costs in the optimisation problem. However, additional construction costs (e.g., formwork and labour) can be incorporated into the cost function $C(\boldsymbol{x})$ if necessary [35,41].

The second objective function σ_{Pviol} is the standard deviation of the probability of limit state violation (P_{viol}) due to STS variability. First, the P_{viol} is calculated for each ground motion suite separately. A limit state violation occurs when the seismic demand obtained from the ith random simulation of the seismic response of the bridge pier at the kth seismic action level, $\theta^{(k)}_{max,i}$, exceeds the corresponding limit state capacity threshold $\theta^{(k)}_{c,i}$. P_{viol} is defined as the mean probability of exceedance across all considered limit states, providing a single unified performance metric over the various seismic action levels. An estimate of P_{viol} is obtained using MCS and can be expressed as:

$$P_{viol} = \frac{1}{l \cdot N} \sum_{k=1}^{l} \sum_{i=1}^{N} I\left(z^{(k)}_i\right) \tag{5}$$

where the outcome of the double summation is the total number of unsuccessful simulations (limit state violations) across all limit states, l is the number of limit states ($l = 4$ in this paper), and N is the total number of random simulations at each limit state. Furthermore, $I(\cdot)$ is a binary indicator defined as:

$$I\left(z^{(k)}_i\right) = \begin{cases} 1 & \theta^{(k)}_{max,i} > \theta^{(k)}_{c,i} \\ 0 & otherwise \end{cases} \tag{6}$$

where $\theta^{(k)}_{c,i}$ is the random realisation of $\theta^{(k)}_{c,d}$ described in Table 1 without applying the uncertainty factor related to ultimate limit states as the uncertainties associated with the limit state capacities are explicitly accounted for through the MCS process.

2.5. Solution strategy

The numerical strategy used to solve the proposed RDO framework is presented in this section. Fig. 1 depicts the flowchart of the solution strategy followed to solve the design optimisation problem. For simplicity of illustration, the flowchart considers either a single-pier bridge or a symmetric bridge with piers of equal height. Accordingly, all piers are assumed to have the same diameter D and identical longitudinal and transverse reinforcement ratios, ρ_l and ρ_w. The solution strategy is described in the following.

Step 1 – Compile a parent ensemble of ground motions. A large ensemble of historical ground motion records is selected from the available qualified strong-motion databases. These records should represent, as much as possible, the seismological characteristics of the region under consideration, including earthquake magnitude, source-to-site distance, tectonic environment, and local site conditions. Relaxing the seismological constraints would increase the RTR variability, while, inversely, enforcing advanced selection criteria, such as spectrum compatibility, would reduce the variability [28].

Table 1
Seismic performance limit states as per *fib* MC2010 and corresponding action levels.

Limit States	OP	IU	LS	NC
$\theta_{c,d}$	Mean value of θ_y	Twice the mean value of θ_y	$\theta_{pl,uk}/\gamma^*_R$ ($\gamma^*_R = 1.35$)	$\theta_{pl,uk}/\gamma^*_R$ ($\gamma^*_R = 1.00$)
Seismic Actions	Frequent; 70% probability of exceedance in service life	Occasional; 40% probability of exceedance in service life	Rare; 10% probability of exceedance in service life	Very Rare; 2~5% probability of exceedance in service life

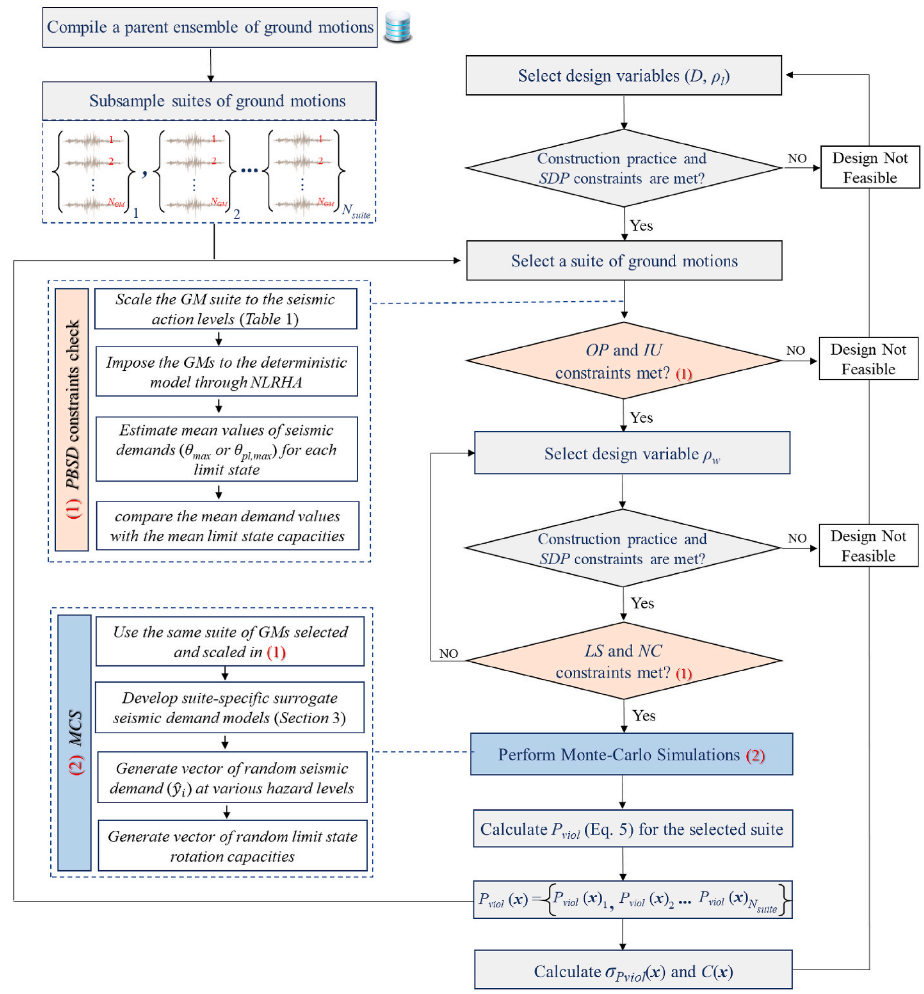

Fig. 1. Flowchart of the solution strategy.

Step 2 – Select the design variables D and ρ_l. The optimiser selects a set of discretised values of the pier design variables (D, ρ_l) to make a design candidate. The selected candidate is checked for *SDP* verifications and construction practice. According to the *fib* MC2010 design approach, only knowledge of D and ρ_l is required to create the pier model and obtain the seismic demands through NLRHAs. Thus, the demand estimation is independent from ρ_w which is treated as a secondary design variable in Step 4.

Step 3 – Select and scale a suite of ground motions. A suite (subset) of at least seven ground motions ($N_{GM} \geq 7$) [7-9] is randomly subsampled from the parent ensemble of records. The records are scaled to represent the required seismic hazard levels using a constant-amplitude scaling procedure which serves as a minimum requirements by major seismic design codes [28] including, i.a., the second-generation Eurocode 8 [9]. Following the recommendations of *fib* MC2010 throughout this study, each horizontal component of a ground motion is treated independently. Each component is scaled such that its 5%-damped elastic response spectrum does not fall below 90% of the target spectrum over the period range $0.2T_1$–$2T_1$, where T_1 is the fundamental period of the bridge.

Step 4 – Check PBSD constraints and determine ρ_w. A *deterministic realisation* of the bridge model is generated using the mean (nominal) values of pier structural capacities (i.e., θ_y and M_y). NLRHAs are performed on the deterministic realisation using the ground motion suite from Step 3. The serviceability (OP and IU) and ultimate (LS and NC) limit states are examined. For the ultimate limit state verification, the design variable ρ_w is determined as the minimum value required to satisfy the SDP constraints and offer adequate flexural deformation capacity ($\theta_{pl,uk}$) and shear resistance (V_{Rd}). At the end, if all design constraints are satisfied, a design candidate is branded as *design solution*. On the other hand, if the optimisation constraints are not satisfied at any point, the design is not feasible and the optimiser returns to Step 2.

Step 5 – Calculate P_{viol} for the design solution through MCS. To include the structural uncertainties, *random realisations* of the bridge pier model are created using statistical moments of the pier structural capacities. Each random realisation is then analysed using the adopted suite of ground motions through NLRHAs to account for the intra-suite RTR variability. Next, the P_{viol} is calculated by comparing the random simulations of structural demand with their corresponding limit state capacity. To improve the computational efficiency of P_{viol} estimation in this step, surrogate seismic demand models may be developed and employed in lieu of full NLRHAs. These surrogates are constructed specifically for the same ground motion suite selected for PBSD in Step 4. The detailed methodology for generating the suite-specific surrogate seismic demand models is subsequently presented in Section 3.

Step 6 – Calculate the optimisation objectives $\sigma_{Pviol}(\boldsymbol{x})$ and $C(\boldsymbol{x})$. Steps 3–5 are repeated using a total number of N_{suite} various ground motion suites subsampled from the parent ensemble of records. Partial replication of ground motion records, meaning that a given record may appear in more than one suite. However, to avoid the dominance of specific records in the MCS, replication may be controlled by ensuring that all ground motions are used an equal number of times across the generated suites. The suite-specific surrogate demand models are subsequently employed within the Monte-Carlo simulation procedure to estimate the corresponding suite-specific P_{viol}. Finally, the collection of P_{viol} values obtained from all suites is used to quantify the optimisation objective $\sigma_{Pviol}(\boldsymbol{x})$.

Step 7 – Repeat steps 2 to 6. The optimiser continues the search of design space (D and ρ_l) until all design candidates are evaluated.

3. Surrogate seismic demand modelling

Surrogate models (metamodels) may be integrated into the MCS phase of the solution strategy to help with computational efficiency of seismic demand estimation through NLRHA. This section outlines the procedure for development and validation of suite-specific surrogate seismic demand models constructed for each seismic action level. These models are not intended to predict response histories or individual nonlinear analysis outcomes. Instead, they are trained to predict the statistical characteristics of the seismic demand, namely its mean and standard deviation, obtained from ensembles of nonlinear analyses.

3.1. Design of experiments

The experimental designs involve combinations of predictor variables used to train the surrogate models. This approach reduces the number of computationally expensive simulations while improving the quality and predictive capabilities of the models [42]. The sequence of experiments is represented as a matrix with each row corresponding to a specific experimental design run. For each run, a set of structure-related predictor variables and an earthquake-related predictor variable are specified.

3.1.1. Structure-related predictor variables

Soltanieh et al. [1] demonstrated the strong correlation between the nominal values of M_y and θ_y, denoted as $(\overline{M_y}, \overline{\theta_y})$, and chord-rotation demands. Therefore, $\overline{M_y}$ and $\overline{\theta_y}$ values are selected as the structure-related predictor variables in this study. These values are directly determined by the design variables (D, ρ_l), using the closed-form equations presented in Ref. [36].

To ensure efficient coverage of the search space with fewer samples, a targeted sampling strategy is adopted. In this approach, m different samples of $(\overline{M_y}, \overline{\theta_y})$ corresponding to (D, ρ_l) are manually selected from the entire space of design candidates. For each sample, Latin hypercube sampling (LHS) is next applied to generate N_{sim} random realisations of the pier moment-rotation model using the statistical moments of $(\overline{M_y}, \overline{\theta_y})$ given by Biskinis & Fardis [36]. This is to take into account the uncertainties associated with structural parameters for each selected

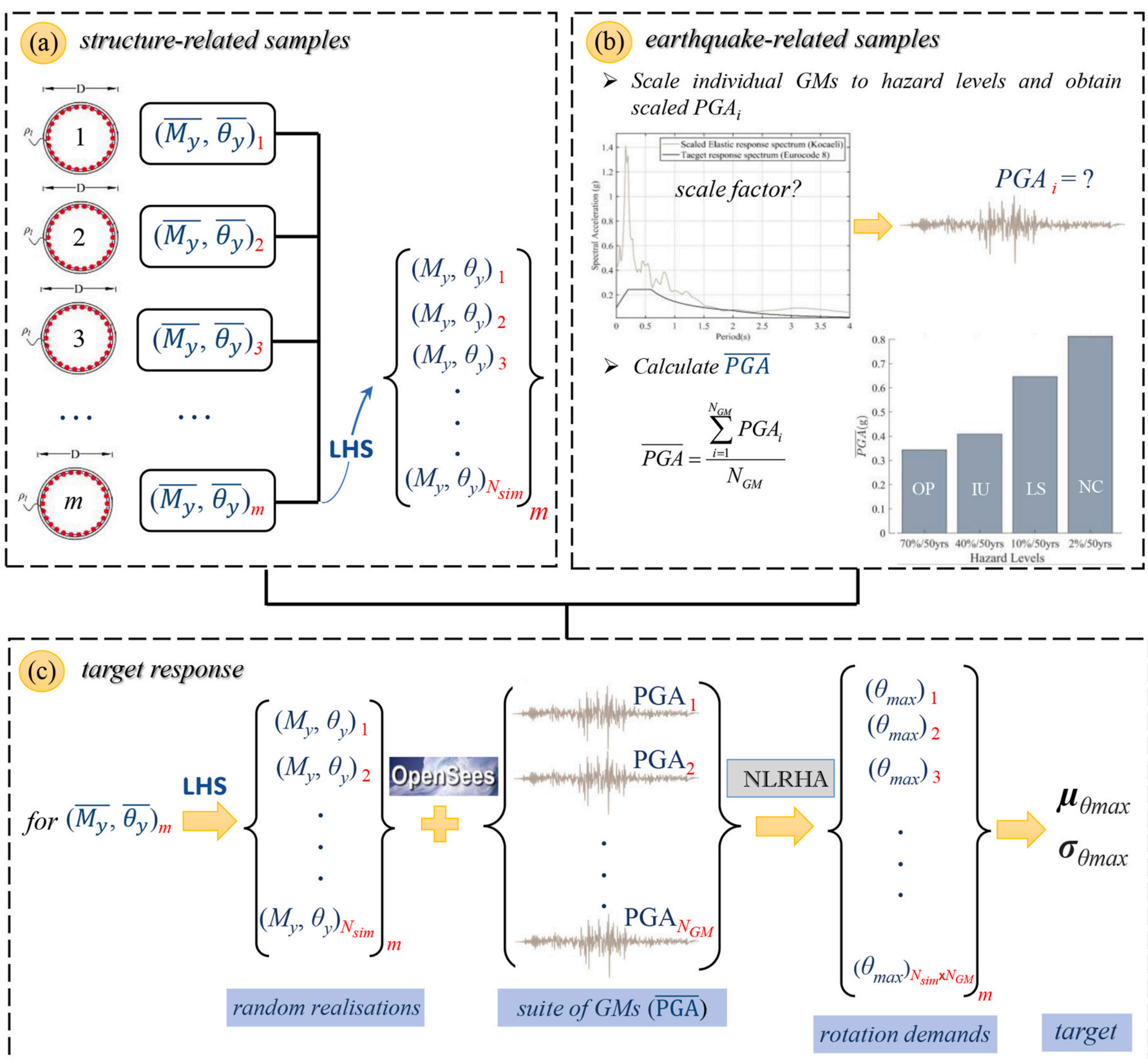

Fig. 2. Schematic illustration of generating experimental designs.

sample. Fig. 2(a) schematically presents the sampling approach.

3.1.2. Earthquake-related predictor variables

For each suite, the average peak ground acceleration (PGA) of scaled ground motions, denoted as $\overline{\mathrm{PGA}}$, is defined as the earthquake predictor variable. First, the geometric mean (PGA_i) of scaled horizontal components (PGA_X and PGA_Y) of each ground motion is calculated. Then, the $\overline{\mathrm{PGA}}$ is estimated as the average of the PGA_i values. Fig. 2(b) schematically illustrates the calculation procedure of $\overline{\mathrm{PGA}}$ at each limit state. The $\overline{\mathrm{PGA}}$ values corresponding to the OP, IU, LS, and NC limit states are denoted as $\overline{\mathrm{PGA}}_{OP}$, $\overline{\mathrm{PGA}}_{IU}$, $\overline{\mathrm{PGA}}_{LS}$, and $\overline{\mathrm{PGA}}_{NC}$, respectively.

In general, PGA has been widely used in surrogate seismic demand modelling for bridges (e.g., Refs. [43,44]). Use of PGA is particularly advantageous in applications where structural properties vary across the analysis domain, such as seismic design optimisation. It should be noted, however, that spectral intensity measures such as $\mathrm{Sa(T_1)}$, which have been commonly recognised as appropriate predictors for bridge surrogate seismic demand modelling (e.g., Refs. [45,46]), may also be adopted as alternatives. In the present study, the surrogate models are specifically intended for integration within a seismic design optimisation framework, where seismic demands are estimated iteratively for numerous bridge pier designs with varying geometric and reinforcement properties. Consequently, the bridge fundamental period varies across candidate designs, and the use of structure-dependent intensity measures would require the earthquake predictor variable to be re-evaluated for each design iteration. This issue was examined in a preliminary study, where it was observed that the use of average $\mathrm{Sa(T_1)}$ did not lead to improved predictive performance compared to average PGA for the considered dataset. Hence, average PGA was adopted as a simple and uniform earthquake predictor for the surrogate seismic demand models, ensuring consistency across all candidate bridge designs throughout the optimisation process.

3.1.3. Estimation of the structural response (target data)

As shown in Fig. 2(c), N_{sim} random realisations of each structure-related sample m are generated and analysed using a suite of N_{GM} ground motions, resulting in $N_{sim} \times N_{GM}$ NLRHAs. This approach ensures that both the RTR variability of ground motions and the uncertainty in structural parameters are captured. The maximum chord-rotation demands at the bridge piers are recorded for each simulation and seismic action level. The mean ($\boldsymbol{\mu}$) and standard deviation ($\boldsymbol{\sigma}$) of these demands (e.g., $\boldsymbol{\mu}_{\theta max}$ and $\boldsymbol{\sigma}_{\theta max}$) are calculated and employed as the target (output) data for training surrogates at each limit state distinctly. The output parameters are defined in Table 2. In this manner, each row of the experimental design matrix consists of ($\overline{M_y}$, $\overline{\theta_y}$, $\overline{\mathrm{PGA}}$) as input variables. For serviceability limit states, the corresponding output variables used for surrogate training are ($\boldsymbol{\mu}_{\theta max}$, $\boldsymbol{\sigma}_{\theta max}$). For ultimate limit states, the output variables are ($\boldsymbol{\mu}_{\theta p,max}$ and $\boldsymbol{\sigma}_{\theta p,max}$). The experimental design matrix is completed by repeating the above-mentioned procedure for all m structural samples.

3.2. Metamodels fitting and accuracy

Three statistical learning techniques are employed in this research for generating surrogate seismic demand models, including Polynomial Response Surface Models (PRSM), Radial Basis Function Networks (RBFN), and Multivariate Adaptive Regression Splines (MARS). These surrogate modelling approaches are well-established in the development of surrogate seismic demand models [43,46] and are consistent with the objectives of the present study. Quadratic PRSMs are conventionally used in engineering applications with acceptable performance in predicting output responses and because of their simplicity, transparency, and closed-form representability. Besides, RBFNs have demonstrated their ability to provide excellent approximations for a wide range of response functions [47,48]. RBFN is a powerful surrogate modelling technique that shares certain similarities with neural networks while possessing distinct characteristics. Among its main advantages are fast training and the ability to generalise well even when relatively small training datasets are available. In addition, MARS is a nonparametric regression approach that does not assume any specific functional relationship between predictor variables and target data [49]. MARS has demonstrated high prediction accuracy due to its adaptive nature and computational efficiency [46]. This method combines piecewise-linear and piecewise-cubic regression techniques. Despite the aforementioned advantages of the selected statistical learning techniques, it is acknowledged that more recent statistical learning techniques, such as gradient boosting machines and other ensemble tree-based methods, could also be employed, particularly when larger datasets are available and more complex models requiring additional hyperparameter tuning can be effectively trained.

Cross-validation is employed to mitigate bias that may arise from the arbitrary selection of training and validation samples [46]. In this research, the repeated random sub-sampling cross-validation procedure [50] is employed. This technique involves randomly selecting 80% of the response data of bridge pier as the training dataset, while the remaining 20% is reserved for validation purposes. Each metamodel is then fitted to the training set, and the predictive accuracy is assessed using the validation set through various goodness-of-fit estimates. This process is repeated multiple times to minimise the variation in the average goodness-of-fit estimate. Two goodness-of-fit measures, namely the adjusted coefficient of determination (i.e., adjusted R-squared) and the root mean square error (*RMSE*), are employed to evaluate the fitting and predictive accuracy of the surrogate models. Adjusted R-squared and *RMSE* provide different perspectives on the performance of a predictive model. Using both adjusted R-squared and *RMSE* to evaluate the accuracy of predictions is an acceptable approach, since these two metrics provide complementary information about performance of the predictive models [46,51].

Table 2
Target parameters for training surrogate models.

Parameters Description	Symbol
Mean of *maximum* chord-rotation demands (θ_{max})	$\boldsymbol{\mu}_{\theta max}$
Standard deviation of *maximum* chord-rotation demands (θ_{max})	$\boldsymbol{\sigma}_{\theta max}$
Mean of *maximum plastic* chord-rotation demands ($\theta_{p,max}$)	$\boldsymbol{\mu}_{\theta p,max}$
Standard deviation of *maximum plastic* chord-rotation demands ($\theta_{p,max}$)	$\boldsymbol{\sigma}_{\theta p,max}$

3.3. Probability distribution of seismic demands

Following the generation of surrogate seismic demand models, the last step involves predicting the structural response distribution for a given design solution. The mean and standard deviation of rotation demands ($\widehat{y}_{\mu|i}$ and $\widehat{y}_{\sigma|i}$) are approximated for individual design solutions using the seismic demand models. These parameters are a function of the nominal values of structural parameters ($\overline{M_y}$, $\overline{\theta_y}$) and $\overline{\mathrm{PGA}}$ values of the selected ground motion suite at each seismic action level.

$$\widehat{y}_{\mu|i} = f\left(\overline{M_y}, \overline{\theta_y}, \overline{PGA}\right), \widehat{y}_{\sigma|i} = g\left(\overline{M_y}, \overline{\theta_y}, \overline{PGA}\right) \tag{7}$$

Upon obtaining the mean ($\widehat{y}_{\mu|i}$) and standard deviation ($\widehat{y}_{\sigma|i}$), probability distribution of rotation demand can be simulated. The simulated rotation demand ($\widehat{y}_i$) under a normal distribution assumption can mathematically be expressed by the following equation [43]:

$$\widehat{y}_i = \widehat{y}_{\mu|i} + N\left[0, \widehat{y}_{\sigma|i}\right] \tag{8}$$

In this equation, the first term ($\widehat{y}_{\mu|i}$) refers to the predicted mean demand values, and the second term represents normal distribution with mean of zero and standard deviation of $\widehat{y}_{\sigma|i}$. Eq. (8) allows to explicitly account for the RTR variability and uncertainties of structural parameters in the probability distribution of seismic demand ($\hat{y}_i$). It is noted that a lognormal (logN) distribution may alternatively be applied to describe the spread of seismic demands.

4. Application of the proposed RDO framework

4.1. Bridge case-study

The bridge case-study, adopted from Bouassida et al. [52], comprises a three-span continuous voided slab deck with intermediate span length of 35 m and end span lengths of 23 m. The top flange width of the superstructure deck is 10 m and consists of a post-tensioned cast-in-situ concrete voided slab. The superstructure is simply supported on the abutments through a pair of bearings allowing free sliding in both horizontal axes without impact with the abutment back-wall [53]. At the interior supports, the superstructure is supported by two similar single-column piers with circular section. The clear height of the piers is 8m, and each pier is supported by a shallow foundation located on firm deposits. At the top, the piers are monolithically connected to the superstructure deck. The bridge pier under consideration is made of C30/37 concrete with characteristic cylinder strength $f_{ck} = 30$ MPa and S500 reinforcing steel ($f_{yk} = 500$ MPa). Except the pier design variables (D, ρ_l, ρ_w), assumed the same for both piers, all other geometrical and mechanical properties of the pier are treated as the design parameters with fixed values. More details regarding geometric properties, deck loading, and mechanical characteristics of the bridge case-study can be found in Bouassida et al. [52].

4.2. Bridge finite element model

A three-dimensional finite element model of the RC bridge is developed in OpenSees [54]. Fig. 3 schematically illustrates the numerical modelling approach adopted in this study. The deck members are modelled using elastic beam-column elements along the centre axis of the deck in the longitudinal direction [55]. The flexural and torsional stiffness of the deck elements are calculated based on the geometric and material characteristics of the section. The uncracked flexural stiffness of the prestressed concrete deck is considered. The torsional stiffness is 50% of the uncracked stiffness. Superstructure mass is distributed and assigned to the deck nodes. The superstructure is assumed to slide freely at the abutment seats. Deck nodes are connected to the piers' nodes at top using rigid links. The pier foundation is assumed to rest on stiff soil and be of such size that foundation compliance could be ignored.

The regions of plastic hinge at the top and bottom of piers are modelled assuming lumped plasticity. The nonlinear material behaviour of plastic hinges is modelled using zero-length rotational spring elements [56]. Furthermore, the uniaxial bilinear Hysteretic material in OpenSees is used to model the bilinear rigid-plastic moment-rotation hysteretic behaviour of the plastic hinges following the recommendations of *fib* MC2010. The remaining length of the pier is assumed to remain elastic and is modelled using the elastic beam-column elements. In both the *fib* and the Eurocode 8 design frames, yield moment M_y, yielding chord-rotation at the member end θ_y, and shear span L_s are the parameters required for modelling the secant stiffness at yield EI_{eff} and the nonlinear behaviour of the plastic hinge length. These parameters are calculated here based on the mechanics-based analytical models developed by Biskinis & Fardis [36] calibrated on the basis of a large number of test results.

4.3. Design variables

The range of design variables (D, ρ_l, ρ_w) selected for the bridge case-study under investigation is between the minimum of (1.0m, 0.5%, 0.25%) and the maximum of (2.5m, 4%, 1.25%) [34,36]. This range is equivalent to a variation of yield moment capacity $\overline{M_y}$ between 4 MNm and 50 MNm, and yield rotation capacity $\overline{\theta_y}$ (i.e., in transverse direction) between 0.015 rad and 0.0075 rad, respectively. For practical (SDP) constraints, the size of longitudinal reinforcement bars ranges between

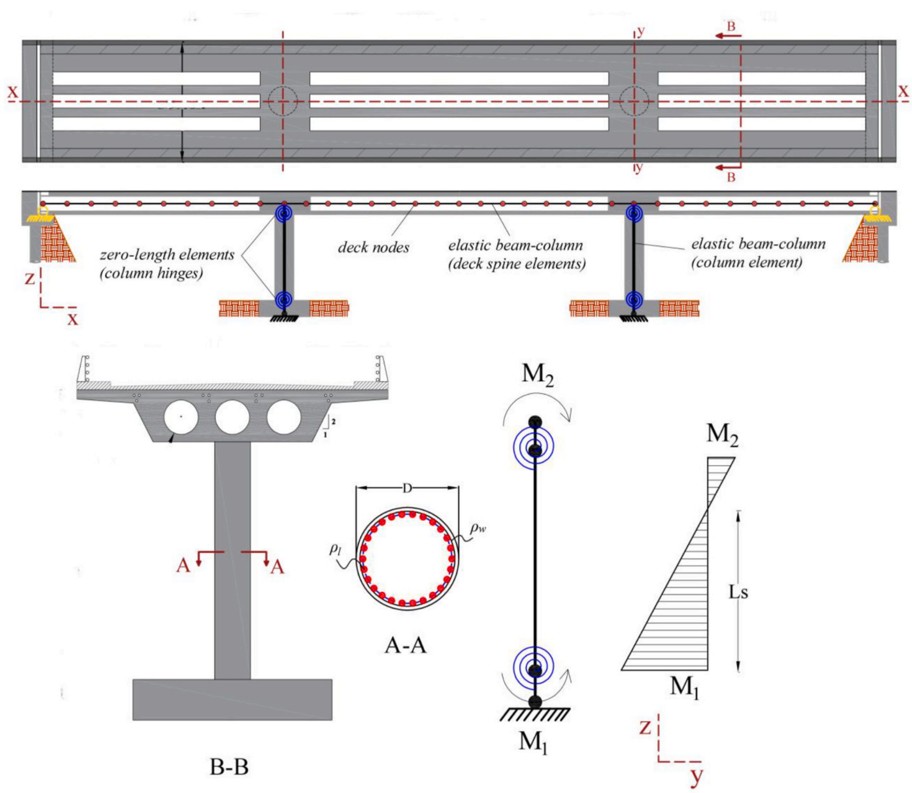

Fig. 3. Schematic view of the bridge finite element modelling approach.

18 mm and 40 mm assuming a single-layer arrangement. Furthermore, the size and arrangement of longitudinal and transverse reinforcement bars are restricted in the present study by construction considerations and structural detailing requirements in *fib* MC2010. The minimum hoop spacing is considered to be no less than 7 mm [34].

4.4. Ensemble of ground motions

To demonstrate the application of the proposed RDO framework in this paper, it is assumed that the minimum code requirements for selecting and scaling ground motion records, as allowed by *fib* MC2010 [7], are adopted to account for RTR variability. In this case, natural records are selected based on the seismological constraints, and constant-amplitude scaling is applied to match the records the code-defined target spectrum at different seismic action levels [28,30]. This approach is applied in the vast majority of actual design studies, also known as the basic requirements by other major seismic design standards including Eurocode 8 [9].

In the aforementioned context, a set of recorded ground motions proposed by Medina and Krawinkler [57] are obtained from the PEER NGA strong motion database. The set represents far-field earthquakes without pulse-like features recorded on stiff soil. It consists of 80 ground motions with M_w between 5.8 and 6.9, R between 13 km and 60 km, and fault rupture mechanisms of strike-slip, reverse-slip, and reverse-oblique. All ground motions are characterised by a shear wave velocity, V_{s30}, between 180 m/s and 360 m/s. The original set is further expanded to 160 records in this study considering the same seismological constraints, in order to compile sufficient records for demonstrating the application of the RDO framework. Fig. 4(a) displays the 5%-damped elastic response spectra of the ground motions in the compiled ensemble. Moreover, Fig. 4(b) presents the mean spectral displacements (μ_s) and their band of one standard deviation ($\pm\sigma_s$) for the original set of 80 ground motions in Ref. [57] and the expanded ensemble of 160 ground motions.

4.5. Ground motion suites

To investigate the STS variability, a total of 28 suites (subsets) of ground motions ($N_{suite} = 28$) are randomly subsampled from the records ensemble. Each suite entails a fixed sample size of $N_{GM} = 40$, which results in 7 replications of each ground motion from the ensemble. This suite size ($N_{GM} = 40$) is adopted to suppress the RTR-induced statistical noise and ensure stable estimates of limit state violation probability within each individual suite. While the magnitude of STS uncertainty is theoretically inversely proportional to suite size, real-world ground motion suites are essentially finite due to the data scarcity satisfying multiple selection criteria as well as the associated computational cost. Consequently, STS variability cannot be eliminated in practice, making it an inherent characteristic of suite-based seismic performance assessment.

Fig. 5(a) & (b) illustrate the unscaled spectral accelerations of horizontal components of an example suite of ground motions with $N_{GM} = 40$. Following the *fib* MC2010 requirements, each individual horizontal component of the selected ground motions are separately scaled to represent the seismic action levels defined in Table 1. The 5%-damped elastic response spectrum defined in Eurocode 8 [8] is adopted as the target spectrum. To construct the target response spectrum for each seismic action level in Table 1, the exceedance probability for a 50-year service life is first converted into equivalent return periods using a Poisson model. The reference target response spectrum is associated with the LS limit state (i.e., 475-year return period), defined according to Eurocode 8 [8] Type I elastic spectrum for Ground Class A, using a reference peak ground acceleration of 0.16g and a 5% viscous damping ratio. For other limit states (OP, IU, and NC), the reference spectrum is scaled to correspond the exceedance probability (return period) using a hazard exponent k of 3.0. The scale factors applied to the selected ground motions vary with the hazard level. In the present study, the mean scale factors for OP and IU limit states are approximately 2.0 and 2.4, while they are 4.4 and 5.6 for LS and NC limit states.

4.6. PBSD constraint checks

The space of design variables is searched through a brute-force approach to ensure that all possible combinations of design variables are evaluated, preventing any potentially optimal solutions from being overlooked. From all feasible combinations of design variables, about 270 candidates successfully satisfy the PBSD constraints related to *fib* MC2010 at various seismic action levels corresponding to OP, IU, LS, and NC limit states as defined in Section 2.3. These are referred to as 'design solutions' throughout this section. Optimisation objectives are calculated only for design solutions as they satisfy the design safety requirements.

4.7. Estimation of P_{viol}

This section describes the procedure of estimating P_{viol} for ground motion suites using surrogate seismic demand models. For brevity, the procedure of developing and validating the surrogates is demonstrated only for the example suite of ground motions whose spectral accelerations are shown in Fig. 5. The same procedure applies for all suites.

4.7.1. Experimental designs (DoE)

A total of $m = 35$ samples of structure-related predictor variables ($\overline{M}_y$, $\overline{\theta}_y$) are selected using a targeted sampling strategy to ensure that

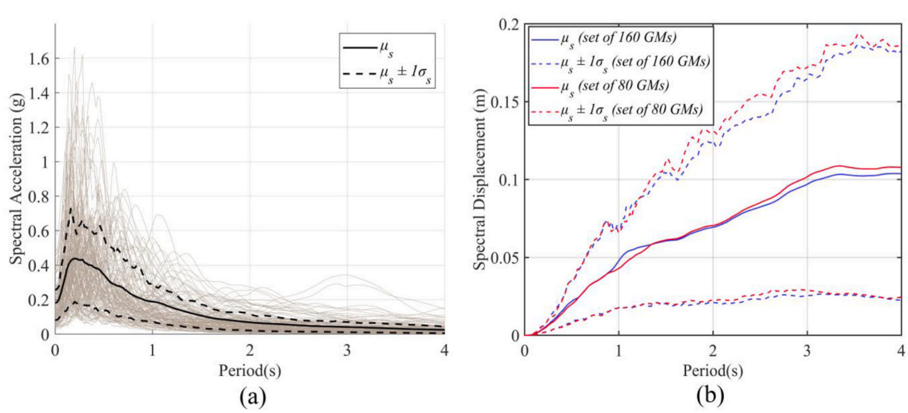

Fig. 4. (a) Spectral accelerations of the ensemble of 160 records, and (b) mean and deviation of spectral displacements for the set of 80 and the expanded set of 160 ground motions.

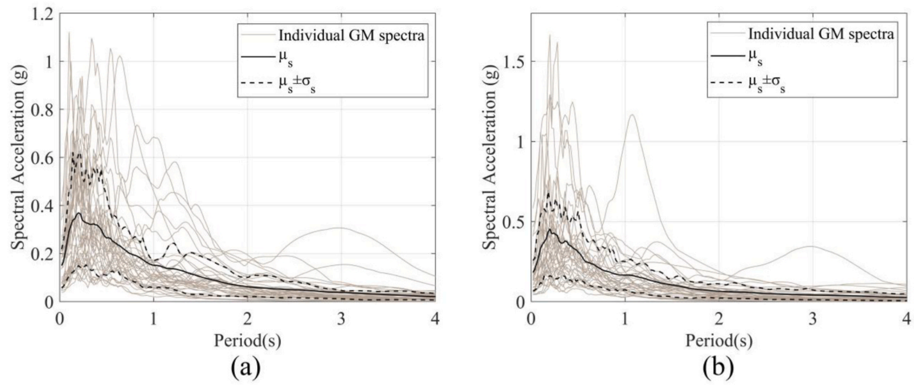

Fig. 5. (a) spectral accelerations (unscaled) related to the 1st horizontal component of ground motion suite (along the bridge X direction), (b) spectral accelerations (unscaled) related to the 2nd component of the ground motion set (along the bridge Y direction).

the range of design variables is uniformly covered. In order to incorporate the uncertainty of structural parameters in seismic response, the mean and *COV*s of the test-to-model ratios for $\overline{M_y}$ and $\overline{\theta_y}$ are adopted from Table 3, and $N_{sim} = 10$ random realisations of the bridge piers are created for each pair of ($\overline{M_y}$, $\overline{\theta_y}$) using the LHS technique. The number of random realisations adopted for each sample was selected based on a sensitivity analysis reported in Refs. [1,58], providing an efficient compromise between statistical confidence and computational cost of MSC simulations.

For each experimental sample, $N_{sim} \times N_{GM} = 10 \times 40 = 400$ NLRHAs are performed at each seismic action level resulting in a total of 1600 NLRHAs across the four limit states. The rotation demands are recorded in both the longitudinal and transverse directions, and the target response statistics, namely, $\boldsymbol{\mu}_{\theta max}$, $\boldsymbol{\sigma}_{\theta max}$, $\boldsymbol{\mu}_{\theta p,max}$, and $\boldsymbol{\sigma}_{\theta p,max}$ (see Table 2) are subsequently estimated. For illustration, consider a representative experimental sample with ($\overline{M_y}$, $\overline{\theta_y}$) = (7084.4 kNm, 0.0116 rad), corresponding to (D, ρ_l) = (1.45m, 1.5%), which yields a fundamental period $T_1 = 1.6$ s in the transverse direction. For this sample, the $\overline{\text{PGA}}$ of the scaled ground motion suite at each seismic action level is: $\overline{\text{PGA}}_{OP} = 0.33$g, $\overline{\text{PGA}}_{IU} = 0.39$g, $\overline{\text{PGA}}_{LS} = 0.62$g, and $\overline{\text{PGA}}_{NC} = 0.78$g. Fig. 6 illustrates the rotation demands against the $\overline{\text{PGA}}$ values associated with different seismic action levels. The $\boldsymbol{\mu}_{\theta max}$ and $\boldsymbol{\sigma}_{\theta max}$ values are calculated for OP and IU limit states, whereas the $\boldsymbol{\mu}_{\theta p,max}$ and $\boldsymbol{\sigma}_{\theta p,max}$ values are estimated for LS and NC limit states considering the plastic part of the rotation demands. Similarly, these quantities are evaluated for all experimental samples to complete the design matrix used for surrogate model training.

4.7.2. Fitting and accuracy of the surrogate models

PRSM, RBFN, and MARS are employed to fit surrogate seismic demand models using training data from the experimental designs. Fig. 7 shows a comparison of the predictive capabilities of the models derived for estimating structural demands at various limit states via the goodness-of-fit measures. This figure indicates the accuracy of metamodels using adjusted R-squared and RMSE for approximating the mean (μ) and standard deviation (σ) of maximum chord-rotation demands recorded along the longitudinal (X) and transverse (Y) direction of the bridge. For example, $\boldsymbol{\mu}_{\theta,X}|_{\text{OP}}$ is the notation for mean value (μ) of the rotation demands θ (abbreviated form of θ_{max}) obtained along the longitudinal axis (X) of the bridge for the OP limit state, and $\boldsymbol{\sigma}_{\theta,Y}|_{\text{IU}}$ is the standard deviation (σ) of the rotation demands obtained along the transverse axis (Y) for the IU limit state.

As shown in Fig. 7, all surrogate models exhibit rather high R-squared (i.e., R-squared greater than 0.7 [46]). Quadratic PRSMs demonstrate rather acceptable R-squared and RMSE values for most of the investigated parameters, despite being the least accurate amongst the three metamodeling techniques. On the other hand, RBFN-based models are found to outperform MARS and PRSM with better goodness-of-fit estimates. In other words, greater R-squared and lower RMSE are obtained using the RBFN models. The maximum RMSE resulted from RBFNs is less than 8% for most cases of target response, which is a fairly acceptable error [51]. This demonstrates superior accuracy in approximating seismic demands, making RBFNs a suitable choice for predicting rotation demands. Nevertheless, it is noted that MARS performs reasonably well and exhibits competitive predictive capabilities, although slightly lower than RBFN. Therefore, RBFNs are utilised to construct the surrogate seismic demand models herein.

Furthermore, a comparative assessment is conducted to calibrate the P_{viol} values approximated through the seismic demand models with those estimated by actual structural analyses. For this purpose, a representative set of design solutions is chosen. The design characteristics of individual design solutions in the representative set are listed in Table 4. The actual rotation demands for this set are captured through actual NLRHAs using the example suite of ground motions in Fig. 5 and compared with the limit state capacities to calculate P_{viol} using Eq. (5). Fig. 8 displays the P_{viol} values obtained from the actual analyses and the surrogate seismic demand models for the set of representative design solutions. In the latter case, the P_{viol} values are calculated through the MCS process using a large number of simulations (10k). In general, it is observed that the prediction error is minimal (typically less than 6%) for the majority of the representative design solutions. A small number of cases (e.g., #26 and #28) exhibit slightly higher discrepancies (up to approximately 10%), which can be attributed to local nonlinear response variations in the actual analyses. Nevertheless, the overall agreement between the surrogate-based and NLRHA-based estimates confirms that the surrogate seismic demand models provide sufficiently accurate predictions of P_{viol}. Moreover, it was found that choosing normal distribution with 95% confidence interval for simulating the vector of seismic demands ($\widehat{y}_i$) (Eq. (8)) at OP and IU, and lognormal (logN) distribution for simulating $\widehat{y}_i$ at LS and NC (where $\theta_{p,max}$ is employed as the *EDP*) result in more precise approximation of P_{viol}.

The use of surrogate models leads to a substantial reduction in the offline computational effort associated with the proposed RDO framework. The offline cost of developing the surrogate seismic demand models in the present study is governed by the number of structural

Table 3
Variation of random parameters: test-to-prediction ratios of mean, median, and *COV* [29].

Test-to-prediction measures	Uncertain Capacity Parameters		
	M_y	θ_y	θ_u
Mean	1.015	1.05	1.03
Median	1.005	1.005	1.00
COV (%)	13.6	31.7	30.3

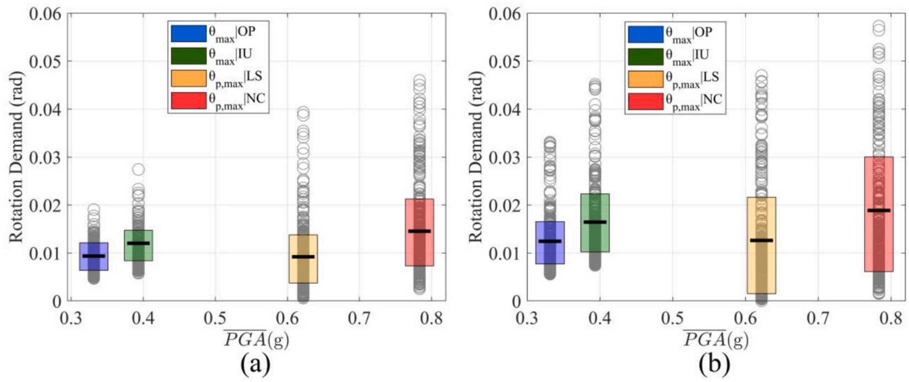

Fig. 6. Rotation demands considering the representative sample (D, ρ_l) = (1.45m, 1.5%) along the (a) longitudinal direction and (b) transverse direction of the bridge.

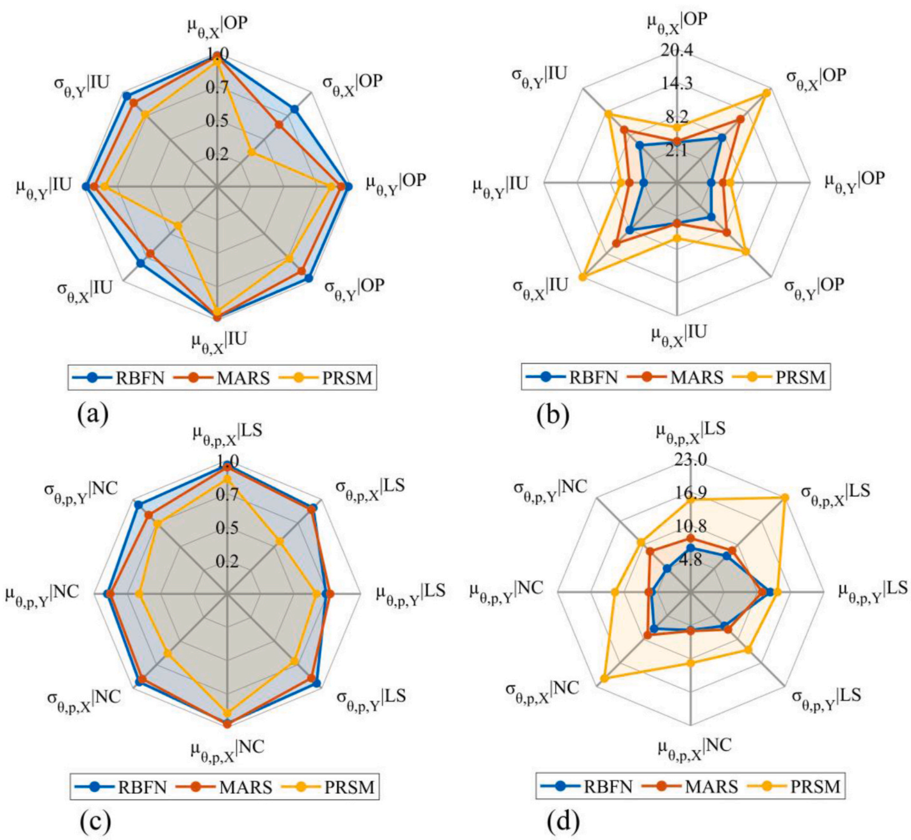

Fig. 7. Approximation accuracy of different metamodeling techniques: (a) adjusted R-square for maximum chord-rotation demands; (b) RMSE (%) for maximum chord-rotation demands; (c) adjusted R-squared for plastic rotation demands; (d) RMSE (%) for plastic chord-rotation demands.

samples selected from the design space (m = 35). Consequently, approximately 1400 NLRHAs ($m = 35 \times N_{sim} = 10 \times 4$ seismic action levels) for each ground motion are required to generate the target response data used for surrogate training. In contrast, a direct NLRHA-based optimisation would require nonlinear analyses for every candidate bridge design considered during the optimisation process. For the present case study, involving more than 200 candidate designs, this corresponds to at least 8000 nonlinear analyses ($200 \times 10 \times 4$) for each ground motion. Therefore, the proposed surrogate modelling strategy reduces the offline computational effort by approximately a factor of five. During the online stage, the surrogate-assisted Monte-Carlo simulation framework still incurs computational cost when evaluating seismic demand statistics and objective functions; however, this cost is several orders of magnitude lower than that associated with direct NLRHAs.

4.8. Optimisation results

Fig. 9 indicates the range of variation in P_{viol} values for the representative set of designs in Table 4. This figure implies that the variation in P_{viol} values due to selecting different suites of ground motions can be significant. For example, the smallest difference between the upper and the lower bounds of the P_{viol} values for a design is given by design #38, i.e., (D, ρ_l, ρ_w) = (2.35m, 2.5%, 0.5%). For this design, the upper bound is 2.8% and the lower bound is 0.5%. On the other hand, the highest difference between the two bounds resulted from design #11, i.e., (D, ρ_l,

Table 4
Design parameter values in the representative set of design solutions.

#	1	2	3	4	5	6	7	8	9	10	11	12	13
D (m)	1.00	1.15	1.15	1.15	1.30	1.30	1.30	1.30	1.30	1.45	1.45	1.45	1.45
ρ_l %	3.50	2.50	3.50	3.50	1.50	2.50	2.50	3.50	3.50	1.50	1.50	2.50	2.50
ρ_w %	0.75	0.75	0.50	0.75	0.75	0.50	0.75	0.50	0.75	0.50	0.75	0.50	0.75
#	14	15	16	17	18	19	20	21	22	23	24	25	26
D (m)	1.45	1.45	1.60	1.60	1.60	1.60	1.60	1.60	1.60	1.75	1.75	1.75	1.90
ρ_l %	3.50	3.50	1.50	1.50	2.50	2.50	3.50	3.50	3.50	1.50	2.50	2.50	1.50
ρ_w %	0.50	0.75	0.50	0.75	0.50	0.75	0.25	0.50	0.75	0.50	0.25	0.50	0.25
#	27	28	29	30	31	32	33	34	35	36	37	38	39
D (m)	1.90	1.90	1.90	2.05	2.05	2.05	2.20	2.20	2.35	2.35	2.35	2.35	2.50
ρ_l %	1.50	2.50	2.50	1.50	1.50	2.50	1.50	2.50	0.50	0.50	1.50	2.50	0.50
ρ_w %	0.50	0.25	0.50	0.25	0.50	0.50	0.50	0.50	0.25	0.50	0.50	0.50	0.25

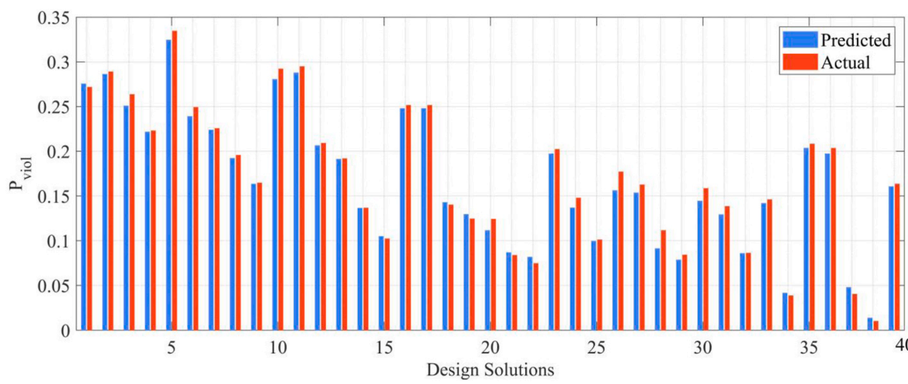

Fig. 8. Predicted and actual values of P_{viol} for the representative design solutions.

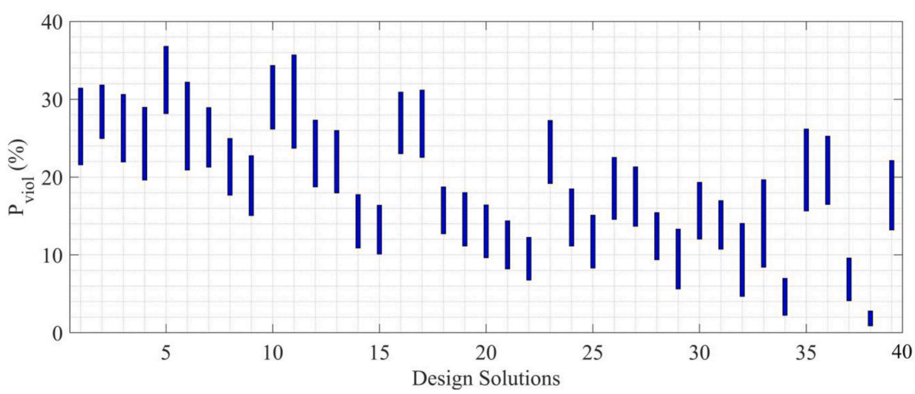

Fig. 9. Variation range of P_{viol} due to ground motion suite variability for the representative set of designs in Table 4.

ρ_w) = (1.45m, 1.5%, 0.075%), where the lower bound of P_{viol} is 23.9% and its upper bound reaches 35.9%.

Fig. 10(a) demonstrates all design solutions and the Pareto-optimal set derived from the RDO method proposed in this study. This figure exhibits the standard deviation of P_{viol}, i.e., σ_{Pviol}, against the total cost of materials, $C(\boldsymbol{x})$, for each design solution. The design characteristics of the Pareto-optimal solutions are listed in Table 5. Amongst these optimal solutions, the most economic (#1) and the most robust (#18) design solutions are (D, ρ_l, ρ_w) = (1.10m, 2.0%, 0.75%) and (D, ρ_l, ρ_w) = (2.25m, 2.5%, 0.5%), respectively. These solutions reflect the trade-off between ductility and strength, where the same performance constraints can be satisfied through increased strength with reduced ductility, or vice versa. All intermediate optimal solutions are referred to as compromise cost-effective solutions.

To highlight the significance of the proposed RDO approach, a cost-effective optimal solution, corresponding to equal emphasis on both optimisation objectives is picked up from the Pareto-optimal set. This design (#5), characterised by (D, ρ_l, ρ_w) = (1.15m, 2.5%, 0.75%), has a material cost 25% greater than the most economic design on the Pareto set but its σ_{Pviol} is about 62% lower than that of the most economical solution, meaning that it is considerably more robust. For this cost-effective solution, for instance, there are several other (non-optimal) design options with similar material costs but greater σ_{Pviol}. The variation range of P_{viol} for these non-optimal solutions is illustrated in Fig. 10 (b) along with that of the optimal cost-effective solution (#5 highlighted in red). As shown in this figure, the P_{viol} variation range for some of these non-optimal solutions can be fairly significant. For example, although the design option with (D, ρ_l, ρ_w) = (1.0m, 3.5%, 1.0%) entails the same material cost as design #5, it shows about 45% higher sensitivity against the STS variability.

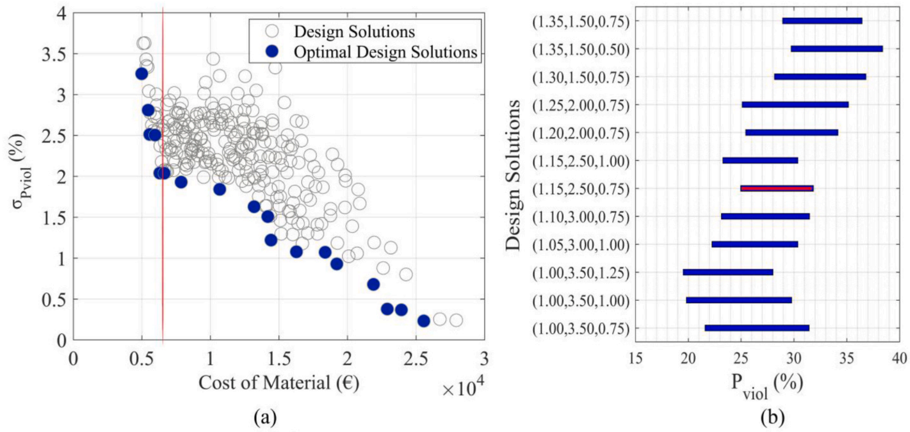

Fig. 10. (a) Dispersion of exceedance probability versus material costs for individual designs and the Pareto-optimal solutions, (b) range of P_{viol} variation for design #5 compared to similar non-optimal solutions.

Table 5
Design characteristics of the Pareto-optimal solutions.

#	1	2	3	4	5	6	7	8	9
D (m)	1.10	1.15	1.25	1.20	1.15	1.10	1.50	1.25	1.65
ρ_l %	2.0	2.0	1.5	2.0	2.5	3.0	1.5	4.0	2.5
ρ_w %	0.75	0.75	0.75	0.75	0.75	1.00	0.50	0.75	0.50
#	10	11	12	13	14	15	16	17	18
D (m)	1.50	1.60	1.60	2.25	2.30	2.25	2.30	2.35	2.25
ρ_l %	3.5	3.0	3.5	1.5	1.5	2.0	2.0	2.0	2.5
ρ_w %	0.75	0.75	0.75	0.50	0.50	0.50	0.50	0.50	0.50

It should be noted that the choice of $N_{suite} = 28$ was found to provide sufficient stability in the estimation of σ_{Pviol}. This was observed during a preliminary convergence study, in which further increases in the number of ground motion suites beyond 24 produced only marginal changes in the estimated value of σ_{Pviol}. Fig. 11 illustrates the convergence of σ_{Pviol} estimate as N_{suite} increases for a number of Pareto-optimal solutions in Table 5, namely design 3, 6, 9, 12, 15, and 18.

It is acknowledged that the case study presented herein is based on far-field ground motions recorded on stiff-soil sites. Different seismological and site conditions, such as near-fault excitations or soft-soil deposits, may lead to different seismic demand characteristics and, consequently, influence the magnitude of STS variability and the associated Pareto-optimal solutions. However, a comprehensive investigation into the influence of ground motion characteristics and site conditions on the proposed optimisation procedure was beyond the scope of the present study.

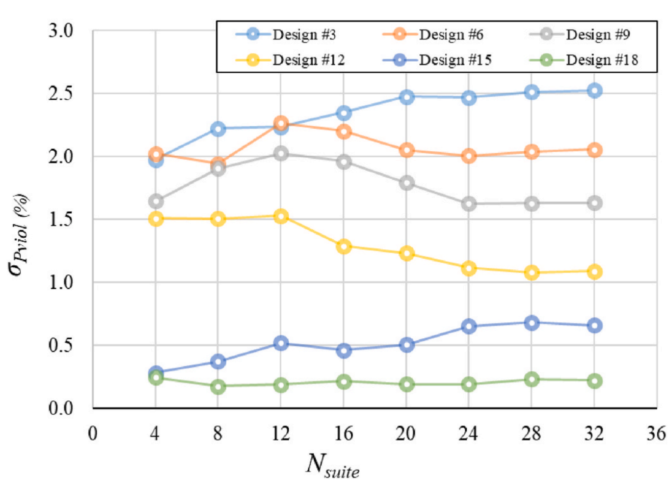

Fig. 11. Variation of against N_{suite}.

4.9. Effects of STS variability

This section compares the Pareto-optimal solutions obtained from the proposed RDO approach (Fig. 10(a)), which include STS variability, with the case where a single suite of ground motions is considered. Considering the example suite of ground motions shown in Fig. 5, P_{viol} is calculated for individual design solutions and minimised along their material costs $C(\boldsymbol{x})$. In other words, a two-objective optimisation is defined to minimise $[C(\boldsymbol{x}), P_{viol}(\boldsymbol{x})]$. Fig. 12(a) shows the Pareto-optimal solutions for this optimisation.

For each Pareto-optimal solution in Fig. 12(a), the σ_{Pviol} value is calculated considering STS variability. Fig. 12(b) illustrates the comparison between the Pareto-optimal solutions obtained from the proposed RDO approach (from Fig. 10(a)) and those obtained from Fig. 12(a). The difference between the Pareto solutions in Fig. 12(b) identifies solutions that are sensitive to STS variability. The maximum difference between the σ_{Pviol} values of the compromise solutions given by the two sets of Pareto solutions can reach up to 60%.

5. Comparison with conventional RDO

The proposed RDO approach in this study can be combined with other optimisation frameworks to support more informed decision-making in code-based PBSD procedures. In this section, the Pareto-optimal solutions obtained from the proposed framework are compared with those obtained from the conventional RDO method defined by Eq. (1). While the proposed RDO promotes solutions that are less sensitive to STS variability, the conventional RDO promotes those that are less sensitive to RTR variability within a single suite of ground motions and at a specific limit state.

The RDO framework defined in the context of PBSD includes

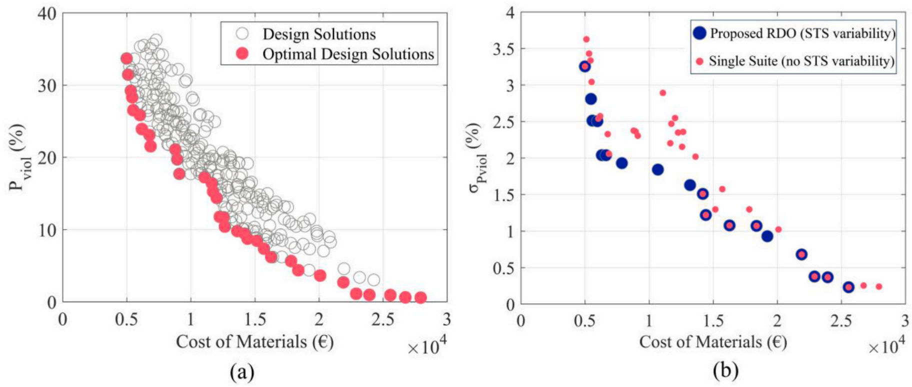

Fig. 12. (a) optimisation for $C(\boldsymbol{x})$ and $P_{viol}(\boldsymbol{x})$ without STS variability, (b) comparison of the Pareto-optimal solutions with and without STS variability.

minimisation of cost $C(\boldsymbol{x})$ and $\sigma_{\theta max}(\boldsymbol{x})$ as described in Eq. (1) [1,18] under the same PBSD constraints defined in Section 2.3. Since the conventional RDO is inherently a suite-specific optimisation framework, the example suite of ground motions in Fig. 5 is adopted for obtaining the Pareto-optimal solutions. These solutions are identified at four different seismic hazard levels corresponding to OP, IU, LS, and NC limit states. For each solution, the σ_{Pviol} values are calculated and plotted against the material costs $C(\boldsymbol{x})$ in Fig. 13. In addition, the Pareto-optimal solutions of the proposed RDO derived from Fig. 10 are plotted in this figure. This figure shows that the σ_{Pviol} values of the compromise Pareto-optimal solutions obtained from the conventional and proposed approach are considerably different. For the selected example suite, the σ_{Pviol} values of the optimal design solutions obtained using the conventional approach are up to 230% of those obtained using the proposed approach. The difference in σ_{Pviol} values may vary across different ground motion suites; however, the conventional RDO consistently results in considerably greater σ_{Pviol} values compared with the proposed RDO approach. This comparison illustrates the benefit of the proposed RDO approach in identifying cost-effective design solutions that are less sensitive to the STS variability due to ground motion suite selection.

6. Conclusions

Existing robust and reliability-based design optimisation approaches account for ground motion record-to-record (RTR) variability. However, the optimal design solutions can still be sensitive to suite-to-suite (STS) variability due to the epistemic uncertainties associated with the selection of ground motion suites for NLRHA, especially when the suite is selected based on the minimum selection and scaling criteria adopted by current seismic design codes.

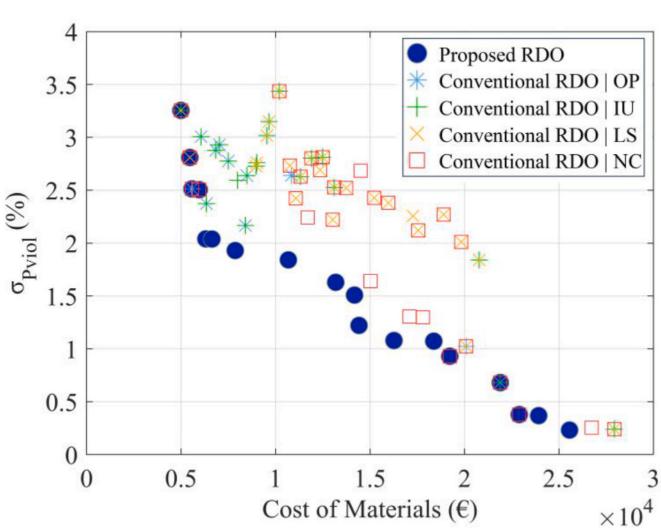

Fig. 13. Comparison between σ_{Pviol} values of the optimal solutions given by the conventional and proposed RDO.

To address the sensitivity of optimal design to STS variability, a novel formulation for robust design optimisation (RDO) of PBSD was developed in this study. In this framework, a two-objective optimisation problem is formulated where the first objective is to minimise the material cost, and the second objective is to minimise the standard deviation of probability of limit state violation (σ_{Pviol}) due to variation in the suite of ground motions.

The application of the proposed RDO framework was demonstrated for a three-span RC bridge with cylindrical piers monolithically connected to the deck. The optimisation results show that the most robust solutions might not be economically reasonable. The most robust design exhibits significantly lower sensitivity to STS variability (over 90%) compared to the economic design, while at the same time, it shows significantly (about 400%) increased cost of materials. This encourages the search for compromise Pareto solutions through a desirability analysis. In this case, a cost-effective solution is found that is only slightly more expensive than the most economic design but about 62% more robust against STS variability. In addition, it was shown that the proposed method could identify compromise Pareto-optimal solutions with about 60% reduced sensitivity against STS variability.

Furthermore, the proposed RDO optimal solutions were compared with those obtained from the conventional RDO approach used in the context of PBSD. It was shown that optimal solutions identified by the conventional RDO, although least sensitive to the intra-suite (RTR) variability, may be markedly sensitive to the STS variability.

To increase the computational efficiency of the proposed framework, surrogate seismic demand models were applied to circumvent the need for computationally demanding NLRHAs associated with seismic demand estimations and calculation of P_{viol}. A feature that distinguishes the surrogate models developed in this study with those of existing studies is their ability to explicitly approximate the standard deviation of seismic demands at various PBSD limit states. Although the use of surrogate models within the RDO framework is optional, it leads to a substantial reduction (approximately to one-fifth for the case study considered) in the offline computational cost associated with surrogate construction. In the online stage, the surrogate-assisted Monte-Carlo simulation framework still involves computational effort but it is considerably lower than performing direct nonlinear response-history analyses. In the case of complex bridge models with more design variables and numerous computationally expensive NLRHAs, surrogate models are even more advantageous for performing the MCS phase of the optimisation solution strategy. Although surrogate models were employed herein to approximate seismic demand statistics, extending the surrogate concept to objective functions or the overall optimisation framework constitutes an interesting direction for future research.

CRediT authorship contribution statement

Soheil Soltanieh: Writing – original draft, Visualization, Methodology, Formal analysis, Conceptualization. **Panagiotis E. Mergos:** Writing – review & editing, Supervision, Methodology, Conceptualization. **Andreas J. Kappos:** Writing – review & editing, Supervision, Methodology.

Declaration of competing interests

The authors declare that they have no known competing financial interests or personal relationships that could have appeared to influence the work reported in this paper.

Acknowledgment

The first author would like to express sincere gratitude for the support of this research through a doctoral scholarship by the School of Science and Technology at City St George's, University of London.

Data availability

Data will be made available on request.

References

[1] Soltanieh S, Mergos PE, Kappos AJ. Robust optimisation of performance-based seismic design of reinforced concrete bridge piers. Earthq Eng Struct Dynam 2025;54(12):3265–80.
[2] Ozsarac V, Monteiro R, Calvi GM. Probabilistic seismic assessment of reinforced concrete bridges using simulated records. Struct Infrastruct Eng 2023;19(4):554–74.
[3] Katsimpini PS, Papagiannopoulos G, Hatzigeorgiou G. Nonlinear analysis of bridges considering soil–structure interaction and travelling wave effects under combined train and near-fault seismic loads. Appl Sci 2024;14(24):11688.
[4] Abarca A, Monteiro R, O'Reilly GJ. Seismic risk prioritisation schemes for reinforced concrete bridge portfolios. Struct Infrastruct Eng 2025;21(1):49–69.
[5] Deb A, Conte JP, Restrepo JI. Comprehensive treatment of uncertainties in risk-targeted performance-based seismic design and assessment of bridges. Earthq Eng Struct Dynam 2022;51(14):3272–95.
[6] Izhar MS, Ansari MI, Umair M. Energy based seismic vulnerability assessment tool for reinforced concrete bridges. Bull Earthq Eng 2024;22(10):5259–97.
[7] *fib [International Federation for Structural Concrete]*. model code for concrete structures 2010. Lausanne: Ernst & Sohn; 2013.
[8] CEN [European Committee for Standardisation] TC250, EN1998-1. Eurocode 8: design of structures for earthquake resistance – Part 1: general rules, seismic actions and rules for buildings. Brussels: CEN; 2005.
[9] CEN [European Committee for Standardisation] TC250, EN1998-1. Eurocode 8: design of structures for earthquake resistance – Part 1-1: general rules and seismic action. Brussels: CEN; 2024.
[10] ASCE [American Society of Civil Engineers]. ASCE/SEI 7-22: *Minimum design loads and associated criteria for buildings and other structures*. Reston, Virginia: ASCE; 2022.
[11] Hassanzadeh A, Moradi S, Burton HV. Performance-based design optimization of structures: state-of-the-art review. J Struct Eng 2024;150(8):03124001.
[12] Yazdani H, Khatibinia M, Gharehbaghi S, Hatami K. Probabilistic performance-based optimum seismic design of RC structures considering soil–structure interaction effects. ASCE-ASME J Risk Uncertainty Eng Syst, Part A Civil Eng 2017;3(2):G4016004.
[13] Zacharenaki AE, Fragiadakis M, Papadrakakis M. Reliability-based optimum seismic design of structures using simplified performance estimation methods. Eng Struct 2013;52:707–17.
[14] Li Y, Conte JP. Probabilistic performance-based optimum design of seismic isolation for a California high-speed rail prototype bridge. Earthq Eng Struct Dynam 2018;47(2):497–514.
[15] Bisadi V, Padgett JE. Explicit time-dependent multi-hazard cost analysis based on parameterized demand models for the optimum design of bridge structures. Comput Aided Civ Infrastruct Eng 2015;30(7):541–54.
[16] Hu S, Zou Y, Gai Y, Huang Z, Song G. Risk-based multiobjective optimal seismic design for RC piers using the response surface method and NSGA-II. Adv Civ Eng 2021;2021(1):8852203.
[17] Taflanidis AA, Beck JL. Stochastic subset optimization for reliability optimization and sensitivity analysis in system design. Comput Struct 2009;87(5–6):318–31.
[18] Lagaros ND, Fragiadakis M. Robust performance-based design optimization of steel moment resisting frames. J Earthq Eng 2007;11(5):752–72.
[19] Bhattacharjya S, Chakraborty S. Robust optimization of linear dynamic system with random parameters under stochastic earthquake excitation. Int J Reliab Qual Saf Eng 2009;16(3):261–79.
[20] Kwag S, Ok SY. Robust design of seismic isolation system using constrained multi-objective optimization technique. KSCE J Civ Eng 2013;17(5):1051–63.
[21] Sextos AG, Katsanos EI, Manolis GD. EC8-based earthquake record selection procedure evaluation: validation study based on observed damage of an irregular R/C building. Soil Dynam Earthq Eng 2011;31(4):583–97.
[22] Hariri-Ardebili MA, Sattar S. Uncertainty and bias in generic ground motion sets used for PBEE. Structures, 57. Elsevier; 2023, November, 105088.
[23] Hariri-Ardebili MA, Sattar S. Uncertainty and bias in fragility estimates by intensifying artificial accelerations. Probab Eng Mech 2023;74:103545.
[24] Skoulidou D, Romao X. Uncertainty quantification of fragility and risk estimates due to seismic input variability and capacity model uncertainty. Eng Struct 2019;195:425–37.
[25] Baker JW, Lin T, Shahi SK, Jayaram N. New ground motion selection procedures and selected motions for the PEER transportation research program. PEER report 2011;3:2011.
[26] Lin T, Harmsen SC, Baker JW, Luco N. Conditional spectrum computation incorporating multiple causal earthquakes and ground-motion prediction models. Bull Seismol Soc Am 2013;103(2A):1103–16.
[27] Bradley BA. A generalized conditional intensity measure approach and holistic ground-motion selection. Earthq Eng Struct Dynam 2010;39(12):1321–42.
[28] Caicedo D, Tomić I, Karimzadeh S, Bernardo V, Beyer K, Lourenço PB. Code-based ground motion selection and scaling for seismic assessment: application to two masonry building case studies. J Build Eng 2025:113558.
[29] Paolucci R, Chiecchio A, Vanini M. Spectrum compatible best matching scenario earthquakes. Soil Dynam Earthq Eng 2024;184:108828.
[30] Caicedo D, Karimzadeh S, Bernardo V, Lourenço PB. Selection and scaling approaches of earthquake time-series for structural engineering applications: a state-of-the-art review. Arch Comput Methods Eng 2024;31(3):1475–505.
[31] Wang L, Hwang JH, Juang CH, Atamturktur S. Reliability-based design of rock slopes—a new perspective on design robustness. Eng Geol 2013;154:56–63.
[32] Pandit B, Babu GS. Reliability-based robust design for reinforcement of jointed rock slope. Georisk 2018;12(2):152–68.
[33] Camacho VT, Horta N, Lopes M, Oliveira CS. Optimizing earthquake design of reinforced concrete bridge infrastructures based on evolutionary computation techniques: V. Camacho et al. Struct Multidiscip Optim 2020;61(3):1087–105.
[34] Sung YC, Su CK. Fuzzy genetic optimization on performance-based seismic design of reinforced concrete bridge piers with single-column type. Optim Eng 2010;11(3):471–96.
[35] Mergos PE. Optimum seismic design of reinforced concrete frames according to Eurocode 8 and fib Model Code 2010. Earthq Eng Struct Dynam 2017;46(7):1181–201.
[36] Biskinis D, Fardis MN. Stiffness and cyclic deformation capacity of circular RC columns with or without lap-splices and FRP wrapping. Bull Earthq Eng 2013;11(5):1447–66.
[37] Fardis MN. Performance-and displacement-based seismic design and assessment of concrete structures in fib Model Code 2010. Struct Concr 2013;14(3):215–29.
[38] Franchin P, Noto F. Reliability-based partial factors for seismic design and assessment consistent with second-generation eurocode 8. Earthq Eng Struct Dynam 2023;52(13):4026–47.
[39] European Committee for Standardization [CEN]. EN 1998-3: Eurocode 8: design of structures for earthquake resistance - Part 3: assessment and retrofitting of buildings. Brussels: CEN; 2005.
[40] Biskinis D, Fardis MN. Cyclic shear resistance for seismic design, based on monotonic shear models in fib Model Code 2010 and in the 2018 draft of Eurocode 2. Struct Concr 2020;21(1):129–50.
[41] Penadés-Plà V, García-Segura T, Yepes V. Robust design optimization for low-cost concrete box-girder bridge. Mathematics 2020;8(3):398.
[42] Fang KT, Li R, Sudjianto A. Design and modeling for computer experiments. Chapman and Hall/CRC; 2005.
[43] Seo J, Linzell DG. Use of response surface metamodels to generate system level fragilities for existing curved steel bridges. Eng Struct 2013;52:642–53.
[44] Shekhar S, Ghosh J. A metamodeling based seismic life-cycle cost assessment framework for highway bridge structures. Reliab Eng Syst Saf 2020;195:106724.
[45] Du A, Padgett JE. Investigation of multivariate seismic surrogate demand modeling for multi-response structural systems. Eng Struct 2020;207:110210.
[46] Ghosh J, Padgett JE, Dueñas-Osorio L. Surrogate modeling and failure surface visualization for efficient seismic vulnerability assessment of highway bridges. Probab Eng Mech 2013;34:189–99.
[47] Schaback R. A practical guide to radial basis functions. Electronic Resource 2007;11:1–12.
[48] Barnett G. A robust RBF-FD formulation based on polyharmonic splines and polynomials. 2015.
[49] Jekabsons G. ARESLab: adaptive regression splines toolbox for Matlab/Octave (ver. 1.10. 3). Latvia: Institute of Applied Computer Systems Riga Technical Univ 2016.
[50] Picard RR, Cook RD. Cross-validation of regression models. J Am Stat Assoc 1984;79(387):575–83.
[51] Seo J. Seismic vulnerability assessment of a family of horizontally curved steel bridges using response surface metamodels. The Pennsylvania State University; 2009.
[52] Bouassida Y, Bouchon E, Crespo P, Croce P, Davaine L, Denton S, Feldmann M, Frank R, Hanswille G, Hensen W, Kolias B. Bridge design to Eurocodes-Worked examples. Work"Bridge Des to Eurocodes 2012:4–6. Vienna.
[53] Bardakis VG, Fardis MN. Nonlinear dynamic v elastic analysis for seismic deformation demands in concrete bridges having deck integral with the piers. Bull Earthq Eng 2011;9(2):519–35.

[54] Mazzoni S, McKenna F, Scott MH, Fenves GL, Jeremic B. Open system for earthquake engineering simulation. Pacific earthquake engineering research center, Berkeley, California. 2006.
[55] Ramanathan KN. Next generation seismic fragility curves for California bridges incorporating the evolution in seismic design philosophy. Georgia Institute of Technology; 2012.
[56] Chandramohan R, Baker JW, Deierlein GG. Quantifying the influence of ground motion duration on structural collapse capacity using spectrally equivalent records. Earthq Spectra 2016;32(2):927–50.
[57] Medina RA, Krawinkler H. Seismic demands for nondeteriorating frame structures and their dependence on ground motions. Stanford University; 2003.
[58] Soltanieh S, Mergos PE, Kappos AJ. Robust performance-based optimum design of reinforced concrete bridge piers. In: 3rd European conference on earthquake engineering & seismology, bucharest, Romania; 2022.